Efficient and Accurate Sampling of the Thermal Neutron Scattering Law in OpenMC

by

Amelia J. Trainer

SUBMITTED TO THE DEPARTMENT OF NUCLEAR SCIENCE AND ENGINEERING IN PARTIAL FULFILLMENT OF THE REQUIREMENTS FOR THE DEGREE OF

MASTER OF SCIENCE IN NUCLEAR SCIENCE AND ENGINEERING

AT THE

MASSACHUSETTS INSTITUTE OF TECHNOLOGY

JUNE 2019

Signature of Author:⎯⎯⎯⎯⎯⎯⎯⎯⎯⎯⎯⎯⎯⎯⎯⎯⎯⎯⎯⎯⎯⎯⎯⎯

Amelia J. Trainer
Department of Nuclear Science and Engineering
May 18, 2019

Certified by:⎯⎯⎯⎯⎯⎯⎯⎯⎯⎯⎯⎯⎯⎯⎯⎯⎯⎯⎯⎯⎯⎯⎯⎯⎯⎯⎯

Benoit Forget
Associate Professor of Nuclear Science and Engineering
Thesis Supervisor

Accepted by:⎯⎯⎯⎯⎯⎯⎯⎯⎯⎯⎯⎯⎯⎯⎯⎯⎯⎯⎯⎯⎯⎯⎯⎯⎯⎯⎯

Michael Short
Assistant Professor of Nuclear Science and Engineering
Chairman, NSE Committee for Undergraduate Students

Efficient and Accurate Sampling of the Thermal Neutron Scattering Law in OpenMC

by

Amelia J. Trainer

Submitted to the Department of Nuclear Science
and Engineering on May 18, 2019 in Partial
Fulfillment of the Requirements for the Degree of
Master of Science in Nuclear Science and
Engineering

ABSTRACT

THIS IS MY ABSTRACT LOCATED IN TITLEPAGE.TEX

Thesis Supervisor: Benoit Forget
Title: Associate Professor of Nuclear Science and Engineering

Thesis Reader: Kord Smith
Title: Korea Electric Power Company (KEPCO) Professor of the Practice of Nuclear Science and Engineering

Acknowledgements

Thanks

Contents

List of Figures

List of Tables

Chapter 1

Introduction

1.1 Motivation

The merit of a nuclear system simulation is heavily dependent on the accuracy of the input nuclear data. Nuclear data (such as cross sections, particle emissions, etc.) is often complicated and highly energy dependent, which poses a challenge for those interested in efficiently simulating the behavior of a nuclear system. Nuclear data is released in "evaluations", which are prepared by statistically combining experimentally measured data with theoretical predictions. The most widely used format for these evaluations is called the Evaluated Nuclear Data File (ENDF) [1]. ENDF files are generally not directly used by nuclear simulations, but are rather preprocessed to account for simulation-specific conditions. In doing so, the ENDF is converted into a more usable form, called "a compact ENDF" (ACE) [2].

Currently, the most widely trusted code used for nuclear data preprocessing is NJOY, which has been developed and maintained at Los Alamos National Lab (LANL) since the early 1970's [3]. It has a large users base and is versatile for many nuclear data related tasks, including resonance reconstruction, Doppler-Broadening, multi-group cross section generation, and the preparation of thermal neutron scattering data. NJOY's capabilities are spread across 24 modules, two of which (LEAPR and THERMR) handle the calculation and representation of thermal scattering from bound moderators. While the accuracy of thermal neutron scattering data can greatly dictate the quality of thermal reactor analysis and safety margin calculations, it remains a difficult problem, due to effects (molecular structure, neutron wavelength, described below) that are not apparent for higher neutron energies.

Both thermal neutron scattering and resonant neutron scattering are highly dependent on incoming neutron energy. However, thermal neutron scattering cross sections must also account for molecular structure, since the energy of the incoming neutron is generally on the order of the molecules' excitation modes (i.e. below 1-10 eV). Excitation of these modes can result in vibration, translation, or rotation of the target. Vibrational modes, also called phonons, are a primary concern when describing neutron scattering in a solid. In addition to the molecular excitation, thermal neutrons data processing is further complicated by considering the long neutron de Broglie wavelength. When a neutron

has energy in the thermal region, its wavelength can be on the order of the interatomic spacing, which allows it to interact with multiple nuclei, as opposed to a single atom [4].

Despite the above complications, a thermal scattering relationship $S(\alpha, \beta, T)$ is constructed to relate unitless neutron momentum and energy exchange (α and β, respectively) with the double differential inelastic incoherent scattering cross section $\sigma(E \rightarrow E', \mu)$. Once $S(\alpha, \beta, T)$, also called the "scattering law", is obtained, the cross section can be obtained using

$$\sigma(E \rightarrow E', \mu) = \frac{\sigma_b}{2k_b T} \sqrt{\frac{E'}{E}} S(\alpha, \beta, T), \tag{1.1}$$

where σ_b is the characteristic bound scattering cross section of the target isotope, and k_b is Boltzmann's constant and T is the temperature. As shown in Eq. 1.1, if $S(\alpha, \beta, T)$ can be accurately obtained, the differential inelastic incoherent scattering cross section $\sigma(E \rightarrow E', \mu)$ is simple to calculate. Thus, the quality of thermal nuclear system modeling is directly tied to the preparation of the scattering law.

1.2 Current Methods of Preparing $S(\alpha, \beta, T)$

1.2.1 Types of Thermal Neutron Scattering

As mentioned in Sec. 1.1, the most widely used code for nuclear data processing is NJOY, which through two of its modules (LEAPR and THERMR) has the ability to prepare thermal scattering data. In particular, LEAPR is used to create a $S(\alpha, \beta, T)$ table, while THERMR tabulates the scattering law into a convenient form for simulations to use. Since LEAPR primarily calculates $S(\alpha, \beta, T)$, it will be of primary focus for the remainder of this section.

Thermal neutron scattering can be broken into elastic and inelastic parts, which can then be further separated into coherent and incoherent parts. Elastic thermal scattering implies no change in neutron energy[1], while inelastic thermal scattering can result in a change of neutron energy that corresponds with an excitation/de-excitation of the target. Excitations can correspond to creation of vibrational modes (phonons), as well as the creation of translational or rotational modes. For a system of particles with randomly distributed spins, coherent scattering consists of interacting wave effects, whereas incoherent scattering consists solely of a sum of non-interacting waves[2].

For materials with randomly distributed crystallites, the form of coherent inelastic scattering nearly equals that of incoherent inelastic scattering. This allows the coherent and incoherent inelastic components to be combined into one inelastic contribution, an

---

[1]Note that elastic thermal scattering differs from generic elastic scattering. In non-thermal elastic scattering, the total kinetic energy is conserved, which means that the neutron could lose energy if it transfers kinetic energy to the target. For thermal elastic scattering, however, the neutron scatters off of a very large molecular system, which means that the target would not gain significant kinetic energy from the neutron, since the effective mass of the scatterer is so high. Thus, elastic thermal scattering implies no change in neutron energy.

[2]Materials such as cold hydrogen that do not have randomly distributed have additional effects, so they have be considered apart from this simple coherent/incoherent discussion.

approximation known as the "incoherent approximation" [3, 4]. Thus, LEAPR separates the scattering calculation into inelastic, coherent elastic, and incoherent inelastic. This project primarily focuses on inelastic scattering, due to its role in representing neutron energy change in a thermal scattering interaction.

1.2.2 Inelastic Thermal Neutron Scattering

Recall from Sec. 1.1 that the double differential inelastic cross section is defined as

$$\sigma\left(E \rightarrow E', \mu\right) = \frac{\sigma_b}{2k_bT}\sqrt{\frac{E'}{E}}S_{n.sym}(\alpha, \beta, T) \tag{1.1}$$

which describes a neutron with incoming energy E scattering with cosine μ into energy E', where σ_b is the target's characteristic bound scattering cross section, k_b is Boltzmann's constant, and T is the temperature. Note that $S_{n.sym}(\alpha, \beta, T)$ is the non-symmetric form of the scattering law, which is related to the symmetric form by

$$S_{sym}(\alpha, \beta, T) = e^{\beta/2}S_{n.sym}(\alpha, \beta, T). \tag{1.2}$$

Dimensionless momentum and energy transfer, α and β respectively, between a neutron and a target of mass number A, are defined as

$$\alpha = \frac{E' + E - 2\mu\sqrt{E'E}}{Ak_bT} \tag{1.3}$$

$$\beta = \frac{E' - E}{k_bT}. \tag{1.4}$$

The symmetric scattering law $S_{n.sym}(\alpha, \beta)$ can be written as an integral across time in units of $\hbar/k_bT$ seconds,

$$S_{n.sym}(\alpha, \beta, T) = \frac{1}{2\pi}\int_{-\infty}^{\infty} e^{i\beta\hat{t}}e^{-\gamma(\hat{t})} \ d\hat{t} \tag{1.5}$$

where

$$\gamma(\hat{t}) = \alpha\int_{-\infty}^{\infty} P(\beta)\left[1 - e^{-i\beta\hat{t}}\right]e^{-\beta/2} \ d\beta \tag{1.6}$$

and

$$P(\beta) = \frac{\rho(\beta)}{2\beta\sinh(\beta/2)}. \tag{1.7}$$

Here, $\rho(\beta)$ is the phonon distribution or excitation frequency spectrum that is characteristic to the material, which normalizes to unity,

$$\int_0^{\infty} \rho(\beta)d\beta = 1. \tag{1.8}$$

Eq. 1.5 uses the Gaussian Approximation, which assumes a Gaussian representation for the correlation function [5]. In addition, the incoherent inelastic scattering form was

equated with that of coherent elastic scattering (incoherent approximation). To facilitate the calculation of Eq. 1.5, LEAPR decomposes the frequency spectrum $\rho(\beta)$,

$$\rho(\beta) = \sum_{j=1}^{\# \text{ osc.}} \omega_j \delta(\beta_j) + \rho_s(\beta) + \rho_t(\beta)) \tag{1.9}$$

into a sum of discrete oscillators (represented by weighted delta-functions $\omega_j \delta(\beta_j)$), a solid-type spectrum $\rho_s(\beta)$, and a translational spectrum $\rho_t(\beta)$. The solid-type spectrum and translational spectrum integrate to ω_s and ω_t, respectively, such that

$$\sum_{j=1}^{\# \text{ osc.}} \omega_j + \omega_s + \omega_t = 1. \tag{1.10}$$

LEAPR uses each component of this decomposed frequency distribution to create a corresponding scattering law $S_{sym,i}(\alpha, \beta, T)$, then convolves these individual scattering laws to retrieve the true scattering relation $S_{n.sym}(\alpha, \beta, T)$.

Solid-Type Continuous Spectra

The solid-type continuous contribution to $S_{n.sym}(\alpha, \beta, T)$, denoted with an (s) superscript, can be calculated by representing Eq. 1.5 as a sum, and using a finite number of terms of that sum to approximate a contribution value. The solid-type continuous spectra depends on the frequency distribution $\rho(\beta)$. Eq. 1.6 can be rewritten as

$$\gamma(\hat{t}) = \alpha \lambda_s - \alpha \int_{-\infty}^{\infty} P(\beta) e^{-\beta/2} e^{-i\beta\hat{t}} \, d\beta. \tag{1.11}$$

where λ_s, known as the Debye-Waller coefficient for the solid-type spectra, is defined as

$$\lambda_s = \int_{-\infty}^{\infty} P(\beta') e^{-\beta'/2} \, d\beta'. \tag{1.12}$$

Thus, the exponential of Eq. 1.11 is

$$e^{-\gamma(\hat{t})} = \sum_{n=0}^{\infty} \left(e^{-\alpha \lambda_s} \frac{1}{n!} \left[\alpha \int_{-\infty}^{\infty} P(\beta') e^{-\beta'/2} e^{-i\beta'\hat{t}} \, d\beta' \right]^n \right) \tag{1.13}$$

where the exponential of the latter term has been represented as a Taylor series. The above can be used in Eq. 1.5, yielding

$$S^{(s)}_{n.sym}(\alpha, \beta, T) = \frac{1}{2\pi} \int_{-\infty}^{\infty} e^{i\beta\hat{t}} \sum_{n=0}^{\infty} \left(e^{-\alpha \lambda_s} \frac{1}{n!} \left[\alpha \int_{-\infty}^{\infty} P(\beta') e^{-\beta'/2} e^{-i\beta'\hat{t}} \, d\beta' \right]^n \right) \, d\hat{t} \tag{1.14}$$

$$= e^{-\alpha \lambda_s} \sum_{n=0}^{\infty} \frac{\alpha^n}{n!} \frac{1}{2\pi} \int_{-\infty}^{\infty} e^{i\beta\hat{t}} \left[\int_{-\infty}^{\infty} P(\beta') e^{-\beta'/2} e^{-i\beta'\hat{t}} \, d\beta' \right]^n \, d\hat{t} \tag{1.15}$$

$$= e^{-\alpha \lambda_s} \sum_{n=0}^{\infty} \frac{1}{n!} [\alpha \lambda_s]^n \mathcal{T}_n(\beta) \tag{1.16}$$

where

$$\lambda_s^n \mathcal{T}_n(\beta) = \frac{1}{2\pi} \int_{-\infty}^{\infty} e^{i\beta \hat{t}} \left[\int_{-\infty}^{\infty} P(\beta') e^{-\beta'/2} e^{-i\beta' \hat{t}} \, d\beta' \right]^n \, d\hat{t}. \tag{1.17}$$

Note that

$$\mathcal{T}_0(\beta) = \delta(\beta) \tag{1.18}$$

and

$$\mathcal{T}_1(\beta) = \frac{1}{2\pi \lambda_s} \int_{-\infty}^{\infty} e^{i\beta \hat{t}} \int_{-\infty}^{\infty} P(\beta') e^{-\beta'/2} e^{-i\beta' \hat{t}} \, d\beta' \, d\hat{t} \tag{1.19}$$

$$= \frac{1}{2\pi \lambda_s} \int_{-\infty}^{\infty} P(\beta') e^{-\beta'/2} \int_{-\infty}^{\infty} e^{i(\beta - \beta')\hat{t}} \, d\hat{t} \, d\beta' \tag{1.20}$$

$$= \frac{1}{\lambda_s} \int_{-\infty}^{\infty} P(\beta') e^{-\beta'/2} \delta(\beta - \beta') \, d\beta' \tag{1.21}$$

$$= \frac{P(\beta) e^{-\beta/2}}{\lambda_s}. \tag{1.22}$$

As shown in Appendix A.1, $\mathcal{T}_n(\beta)$ can be attained using a convolution integral,

$$\mathcal{T}_n(\beta) = \int_{-\infty}^{\infty} \mathcal{T}_1(\beta') \mathcal{T}_{n-1}(\beta - \beta') \, d\beta'. \tag{A.8}$$

Solving the solid-type, continuous contribution to $S_{n.sym}(\alpha, \beta, T)$ can be done by computing $\mathcal{T}_i(\beta)$ for i from 1 to a sufficiently large value of n. These $\mathcal{T}_i(\beta)$ values can be used in the Eq. 1.16, which directly contributes to $S_{n.sym}(\alpha, \beta, T)$.

Discrete Oscillator

Shown in Fig. 1.1 is the phonon distribution for H in H_2O, as calculated by [6]. Often, vibrational modes appear as sharp peaks in the frequency distribution, and can be treated as a weighted delta functions, $\omega_i \delta_i(E)$. The contribution to the scattering law from oscillator i is

$$S_{n.sym}^{(i)}(\alpha, \beta) = e^{-\alpha \lambda_i} \sum_{n=-\infty}^{\infty} \delta(\beta - n\beta_i) \, \mathrm{I}_n \left[\frac{\alpha w_i}{\beta_i \sinh(\beta_i/2)} \right] e^{-n\beta_i/2} \tag{1.23}$$

where the corresponding Debye-Waller coefficient is

$$\lambda_i = w_i \frac{\coth(\beta_i/2)}{\beta_i} \tag{1.24}$$

and $\mathrm{I}_n(x)$ is the modified Bessel function of the first kind. When combining a continuous, solid-type spectrum with discrete oscillators, the total Debye-Waller coefficient is simply the sum,

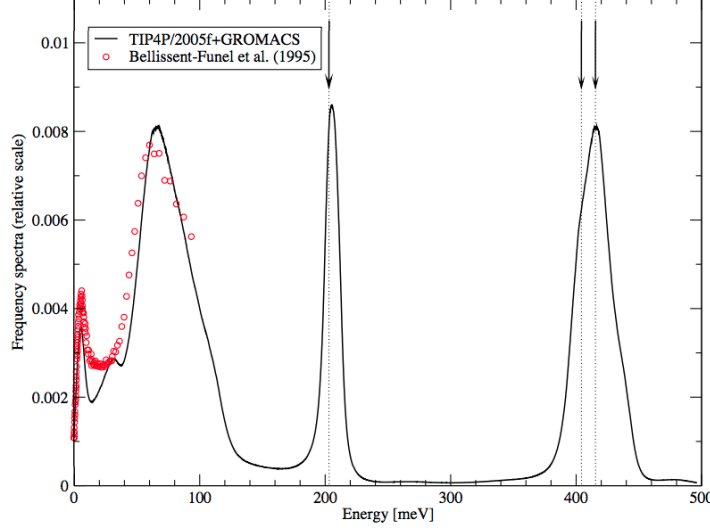$$\lambda = \lambda_s + \sum_{i=1}^{N} \lambda_i \tag{1.25}$$

13

Figure 1.1: Phonon Distribution for H in H_2O [6]. The red points and the arrows represent measured data against which to compare the calculated spectrum. Of particular interest are the two peaks near 200 and 400 meV, which are approximated in LEAPR as discrete oscillators.

where there are N oscillators considered. Combining all the factors in Eq. 1.23 without a β term leaves us with

$$S_{n.sym}^{(i)}(\alpha, \beta) = \sum_{n=-\infty}^{\infty} A_{i,n}(\alpha)\delta\left(\beta - n\beta_i\right) \tag{1.26}$$

where $A_{i,n}(\alpha)$ is defined as

$$A_{i,n}(\alpha) = e^{-\alpha\lambda_i} I_n \left[\frac{\alpha\omega_i}{\beta_i \sinh(\beta_i/2)}\right] e^{-n\beta_i/2}. \tag{1.27}$$

Using Eq. 1.23 or Eq. 1.26, the contribution that an individual oscillator has to the total scattering law is rather simple to compute. Once computed, it must be convolved with the existing scattering law. Consider an example where two discrete oscillators contributions, $S_{n.sym}^{(1)}$ and $S_{n.sym}^{(2)}$, are being combined to a scattering law contribution from solid type spectrum $S_{n.sym}^{(s)}$.

$$S_{n.sym}^{(s,1)}(\alpha, \beta) = \int_{-\infty}^{\infty} S_{n.sym}^{(1)}\left(\alpha, \beta'\right) S_{n.sym}^{(s)}\left(\alpha, \beta - \beta'\right) d\beta' \tag{1.28}$$

$$= \int_{-\infty}^{\infty} \sum_{n=-\infty}^{\infty} A_{1,n}(\alpha)\delta\left(\beta' - \beta_1\right) S_{n.sym}^{(s)}\left(\alpha, \beta - n\beta'\right) d\beta' \tag{1.29}$$

$$= \sum_{n=-\infty}^{\infty} A_{1,n}(\alpha) S_{n.sym}^{(s)}\left(\alpha, \beta - n\beta_1\right) \tag{1.30}$$

14

$$S_{n.sym}^{(s,1,2)}(\alpha,\beta) = \int_{-\infty}^{\infty} S_{n.sym}^{(2)}(\alpha,\beta')\, S_{n.sym}^{(s,1)}(\alpha,\beta-\beta')\, d\beta' \tag{1.31}$$

$$= \int_{-\infty}^{\infty} \sum_{m=-\infty}^{\infty} A_{2,m}(\alpha)\delta\left(\beta'-m\beta_2\right) S_{n.sym}^{(s,1)}(\alpha,\beta-\beta')\, d\beta' \tag{1.32}$$

$$= \sum_{m=-\infty}^{\infty} A_{2,m}(\alpha) S_{n.sym}^{(s,1)}(\alpha,\beta-m\beta_2) \tag{1.33}$$

$$= \sum_{m=-\infty}^{\infty} A_{2,m}(\alpha) \sum_{n=-\infty}^{\infty} A_{1,n}(\alpha) S_{n.sym}^{(s)}(\alpha,\beta-n\beta_1-m\beta_2) \tag{1.34}$$

Translational Spectra

Thermal neutron scattering off of some materials, especially gasses and liquids, can be modeled by considering a solid-type, continuous spectrum, combined with a diffusive term. For liquid moderators, LEAPR makes use of the "effective width model" [7]. The effective width model defines the translational contribution to the scattering law as

$$S_{n.sym}^{(t)}(\alpha,\beta) = e^{[2c^2 w_t \alpha - \beta/2]} \frac{2cw_t\alpha\sqrt{c^2+.25}}{\pi\sqrt{\beta^2+4c^2w_t^2\alpha^2}} K_1\left\{\sqrt{c^2+.25}\sqrt{\beta^2+4c^2w_t^2\alpha^2}\right\} \tag{1.35}$$

with the phonon distribution is defined as

$$\rho(\beta) = w_t \frac{4c}{\pi\beta}\sqrt{c^2+.25}\sinh(\beta/2)K_1\left\{\sqrt{c^2+.25}\beta\right\} \tag{1.36}$$

where w_t is the translational weight, c is the diffusion constant, and K_1 is the modified Bessel function of the second kind.

For gas moderators, and even some liquid moderators, the free gas approximation can be used as an alternative to the effective width model,

$$S_{n.sym}^{(t)}(\alpha,\beta) = e^{-\beta}\frac{1}{\sqrt{4\pi w_t\alpha}}\exp\left[-\frac{(w_t\alpha-\beta)^2}{4w_t\alpha}\right]. \tag{1.37}$$

Once the translational contribution to the scattering law is calculated, it is convolved with the other contributions to obtain the total $S_{n.sym}(\alpha,\beta)$.

1.3 Areas of Improvement

1.3.1 Input Phonon Distribution Approximations

Just to let you know, I intend to address the δ function approximation.

1.3.2 Sampling from $S(\alpha,\beta,T)$

Similarly, I'll let you know here that sampling can be a tough problem with $S(\alpha,\beta)$, so we'll address Pavlou's paper.

Chapter 2

Accurate Representation of Phonon Distributions

2.1 Discrete Oscillator Approximation

The LEAPR module of NJOY, which is used to prepare thermal scattering data in the form of the scattering law, $S(\alpha, \beta, T)$, often approximates peaks in the phonon spectra as discrete oscillators, and models them as weighted δ-functions. In the event that a user would want to avoid this approximation, and instead apply the continuous phonon distribution treatment to those selected areas, it is crucial to verify agreement between these two methods. To test this, a simplified model for H in H_2O is used, which is modeled after Test Problem #9 in the NJOY 2016 release [3].

2.1.1 Problem Specifications

The test case used for this discrete oscillator discussion depicts a simplified H in H_2O model. The water is comprised of H-1 and O-16, and is held at $T = 296$ K. An input phonon spectrum is used for the solid-type continuous model, and two discrete oscillators are used to represent higher energy peaks. The phonon distribution and discrete oscillators, which are gotten from Test #9 in NJOY-2016, are plotted in Fig. 2.1 [3].

The continuous phonon spectrum is defined as $\rho(\beta) = \rho(\Delta E/k_bT)$ for ΔE spanning from 0-0.16575 eV, where the energy grid is uniformly spaced in increments of 0.00255 eV. No translational/diffusive contribution is considered ($\omega_t = 0$). The continuous weighting ω_s is set to 0.5, and the discrete oscillator energies and weights are provided in Table 2.1. Note that the listed weights satisfy the normalization requirement stated in Eq. 1.10.

Table 2.1: Energies and Weights for δ functions used in NJOY 2016 Test Problem 9

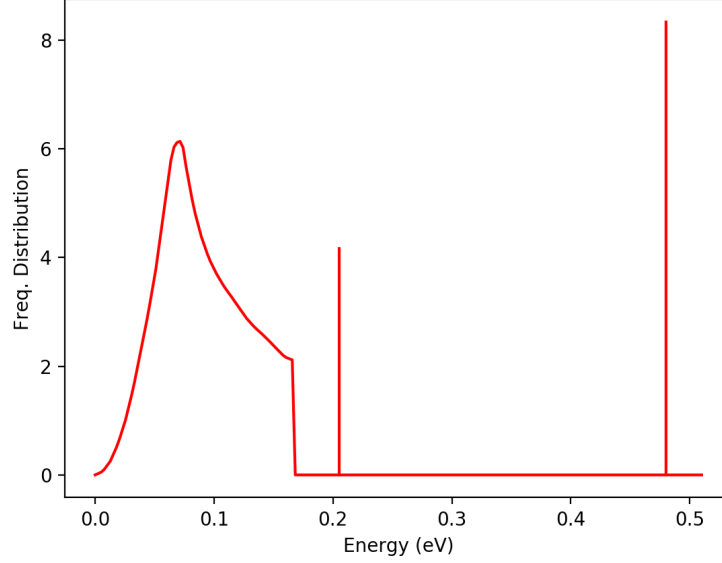| Energy (eV)	Weighting
0.205	0.166667
0.480	0.333333

Figure 2.1: The phonon distribution for NJOY 2016 Test Problem 9 is shown above. It contains a continuous contribution, shown on the lower energy region, and two δ functions to approximate the higher energy peaks. The δ functions are of arbitrary height relative to the continuous spectrum.

2.1.2 Compatible α, β Values

Recalling the definitions of α and β that were stated in Eq. 1.3 and Eq. 1.4, respectively, it is apparent that not all (α, β) pairs are physically compatible. Setting $\mu = \pm 1$ gives the minimum and maximum α values, respectively,

$$\alpha_{max,min} = \frac{E' + E \pm 2\sqrt{E'E}}{Ak_bT}.$$
(2.1)

After defining E' in terms of β and rearranging, this becomes

$$\alpha_{max,min} = \frac{(\beta k_bT + E) + E \pm 2\sqrt{(\beta k_bT + E)E}}{Ak_bT}$$
(2.2)

$$= \frac{\left(\sqrt{\beta k_bT + E} \pm \sqrt{E}\right)^2}{Ak_bT}$$
(2.3)

which means that, for a given β, the valid α range is

$$\frac{\left(\sqrt{\beta k_bT + E} - \sqrt{E}\right)^2}{Ak_bT} \leq \alpha \leq \frac{\left(\sqrt{\beta k_bT + E} + \sqrt{E}\right)^2}{Ak_bT}.$$
(2.4)

This relationship in Eq. 2.4 is plotted in Fig. 2.2, where an initial energy $E = 1$ eV is assumed, and the scattering material is water at $T = 296$ K. In all subsequent discussions, only α and β values that satisfy the requirement in Eq. 2.4 for $E = 1$ eV will be presented. This restricts the conclusions to include more physically meaningful values.
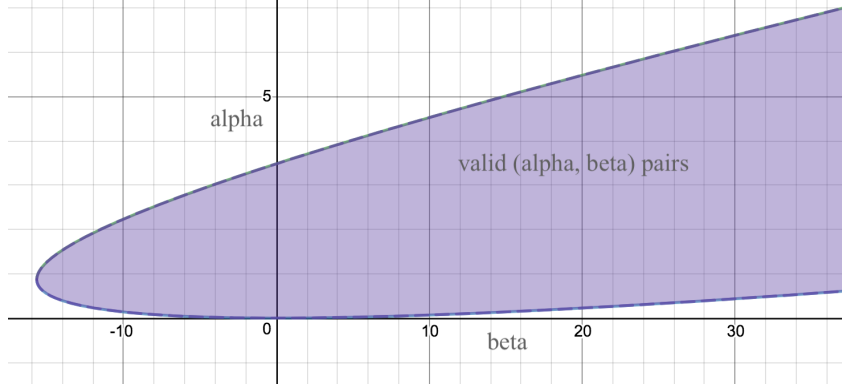
Figure 2.2: Valid α range, given β values, for 1 eV neutron scattering off of water at 296 K. This illustrates the behavior defined in Eq. 2.4.

2.2 Representing Discrete Oscillators as Continuous Points

In order to allow users to avoid the δ function approximation that is commonly used in NJOY's LEAPR module, it is crucial to demonstrate similar behavior between how the solid-type, continuous treatment vs. discrete oscillator treatment processes sharp peaks. The problem specifications detailed in Sec. 2.1.1 are considered, and the discrete oscillators are represented as thin triangles in the continuous spectrum. To allow for more flexible analysis, LEAPR's source code was translated from Fortran to C++. After presenting the phonon spectra used for the oscillator-triangle analysis, the results of the translated C++ LEAPR vs. legacy Fortran LEAPR are shown, for the simple H in H$_2$O model discussed in Sec. 2.1.1.

2.2.1 Replacing Discrete Oscillator δ Functions as Triangles

To verify that discrete oscillator treatment can be replicated by using increasingly thin triangles, each triangle must integrate to the weight of its corresponding δ function. Triangles of various widths (2,4,6,8, and 10 grid spaces) are used to replace both δ functions, and are plotted in Fig. 2.3. Additionally, a close-up of the 0.204 eV oscillator region is provided to illustrate a discrepancy between the triangle and oscillator locations. NJOY requires any continuous phonon distribution to be provided with respect to a uniformly-spaced energy grid. Thus, in Fig. 2.3, the centers of the triangles are not necessarily equal to the exact location of the δ functions that are specified in Table. 2.1. As a result of the discrepancy between discrete oscillator location and triangle center location, the oscillators energies are shifted slightly to align better with the $\Delta E = 0.00255$ eV grid to which NJOY is restricted. The δ function parameters presented in Table. 2.1 are amended to those in Table. 2.2. By slightly shifting the locations of the oscillators so that they are aligned with the triangles' grids, Fig. 2.3 becomes Fig. 2.4. The oscillator energies detailed in Table 2.2 are the problem specifications used for the remainder of this discussion.
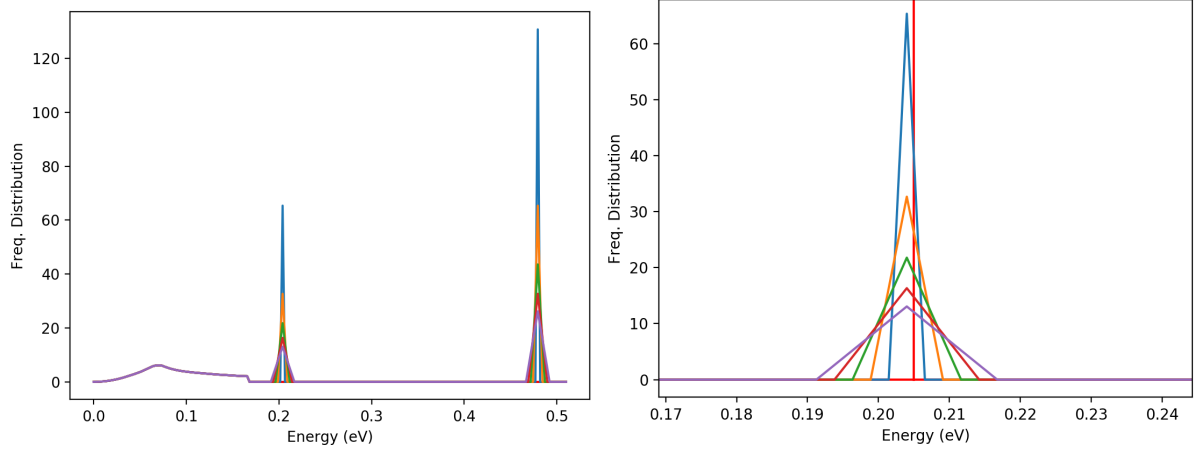
Figure 2.3: Phonon Distribution for H in H_2O, with oscillators replaced with phonon distribution triangles of various widths. The area under each triangle integrates to its corresponding δ function weight ω_i, and the lower energy continuous component integrates to the solid-type weight ω_s. A close-up of the 0.204 eV oscillator is provided. Note that due to the continuous spectrum being defined on a uniform grid, the triangles are not perfectly aligned with the δ function.

Table 2.2: Energies and Weights for δ functions, Amended to Align with Energy Grid

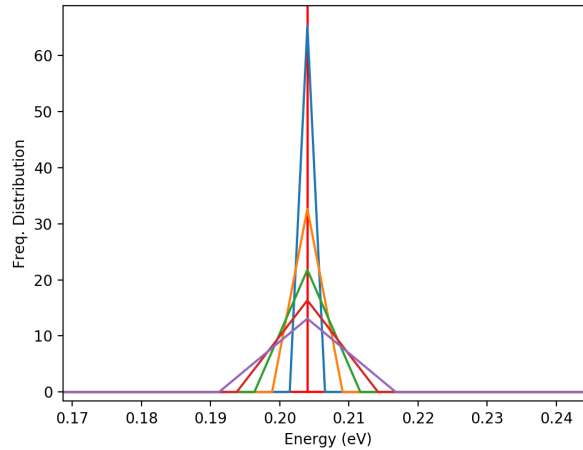| Energy (eV)	Weighting
0.204	0.166667
0.4794	0.333333

Figure 2.4: Phonon distribution for H in H_2O, with triangles approximating the oscillators. The oscillator locations are shifted to the locations listed in Table 2.2, so as to account for the offset due to restrictions in the $\rho(E)$ grid.

2.2.2   Equivalence of Revised-LEAPR to Legacy-LEAPR

NJOY's LEAPR module was translated from Fortran to C++, so as to provide flexibility in later analysis. To use the translated code for analysis requires confidence that it adequately replicates the behavior of the legacy code. To illustrate their compared behavior, Fig. 2.5 contains $S(\alpha, \beta)$ as it was calculated using both the original and the translated LEAPR code. Note that the for nearly all α, β values shown, the two datasets are virtually indistinguishable from each other.
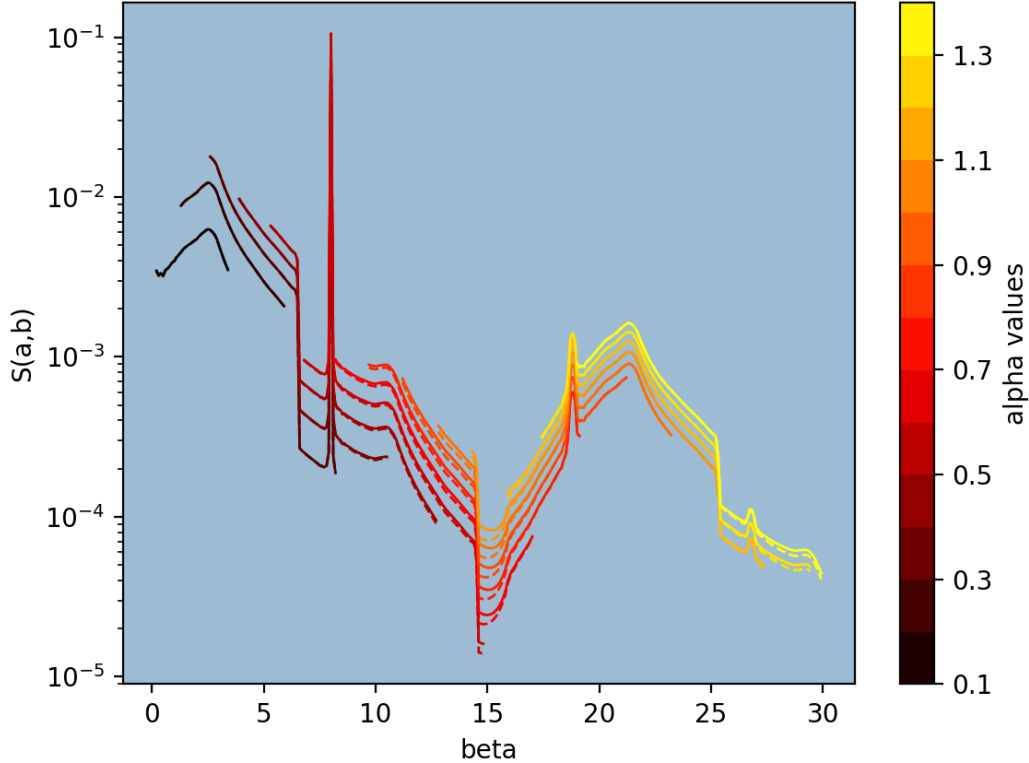

Figure 2.5: Comparison of Translated vs. Legacy LEAPR, using a simple H in H_2O model. Translated and legacy LEAPR are represented using dotted and dashed lines, respectively. Note the sharp peaks that characterize the $S(\alpha, \beta)$ spectrum, which correspond to the summation values in Eq. 1.34, and are identified in Table 2.3.

Fig. 2.6 shows the percent error and the absolute relative error between the $S(\alpha, \beta)$ values produced by the translated and original LEAPR, that were plotted in Fig. 2.5. Notice that the percent error is significantly lower in the β regions where $S(\alpha, \beta)$ is of reasonable size. Thus, the translated version of LEAPR is considered an adequate tool for processing thermal data for the following discussion. However, conclusions drawn using the translated LEAPR will be verified alongside those drawn from the legacy LEAPR. Note that the translated LEAPR was also tested against legacy LEAPR with other cases considered.
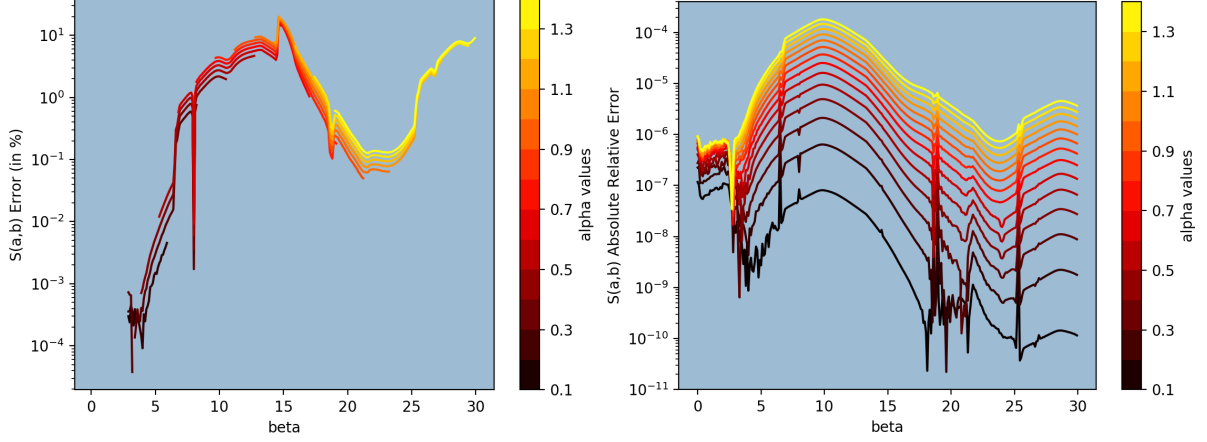
Figure 2.6: Comparison of translated vs. legacy LEAPR, for test #9, with the percent error plotted. Note that large percent error is paired with small absolute error, and is generally of negligible consequence.

Features of $S(\alpha, \beta)$

Fig. 2.5 contains many sharp peaks, at specific β values. Using the material temperature $T = 296$ K and the definition of β from Eq. 1.4, these peaks are converted to eV. The peak locations, both β and eV values, are presented in Table 2.3. Included in Table 2.3

Table 2.3: Locations of Peaks in $S(\alpha, \beta)$ Spectrum that Arise From Oscillator Behavior. This includes some of the main peaks in Fig. 2.5, their corresponding energy values, and the physical reason for the peak.

β Locations of Peaks	ΔE Value (eV)	Origin
7.99	0.204	E_1
10.79	0.275	$E_2 - E_1$
15.99	0.407	$E_1 + E_1$
18.79	0.479	E_2
26.79	0.683	$E_1 + E_2$

are the physical reasons for each of these main peaks shown. Recall Eq. 1.34,

$$S_{n.sym}^{(s,1,2)}(\alpha, \beta) = \sum_{m=-\infty}^{\infty} A_{2,m}(\alpha) \sum_{n=-\infty}^{\infty} A_{1,n}(\alpha) S_{n.sym}^{(s)}(\alpha, \beta - n\beta_1 - m\beta_2) \qquad (1.34)$$

which illustrates the form of the scattering law, when the results of a continuous spectrum is combined with those of two oscillators, located at β_1 and β_2. This indicates the importance of β values that are integer, linear combinations of oscillator locations β_1 and β_2.

21

2.3 $S(\alpha, \beta)$ Response to Continuous vs. Discrete Oscillator Representation

2.3.1 $S(\alpha, \beta)$ Response to Thin Triangle vs. Oscillator

The phonon distributions presented in Fig. 2.4 are input into LEAPR, and the resultant $S(\alpha, \beta)$ is collected. This is compared against the $S(\alpha, \beta)$ grid that is resultant of the typical discrete oscillator representation for the higher end of the H in H$_2$O frequency distribution (i.e. the representation shown in Fig. 2.1). As mentioned in Sec. 2.1.1, the phonon grid is defined with a uniform energy spacing of $\Delta E = 0.00255$ eV, which means that the thinnest triangle available has a total width of $2 \times \Delta E = 0.0051$ eV. For the remainder of Sec. 2.3.1, this minimum-width triangle will be the only triangle of focus. In Sec. 2.3.2, the effects of changing triangle width will be explored.

Fig. 2.7 shows the $S(\alpha, \beta)$ grids generated by translated LEAPR, using both the discrete oscillator and the thin triangle phonon representation. The $S(\alpha, \beta)$ grid is plotted against β for various α values. Note that the peaks near 16, 18, and 26 eV are significantly more pronounced in Fig. 2.7 than they were in Fig. 2.5. To better see the effects that continuous vs. discrete oscillator representation has on $S(\alpha, \beta)$ behavior near peaks, enlarged views of these peak regions are provided in Fig. 2.8.
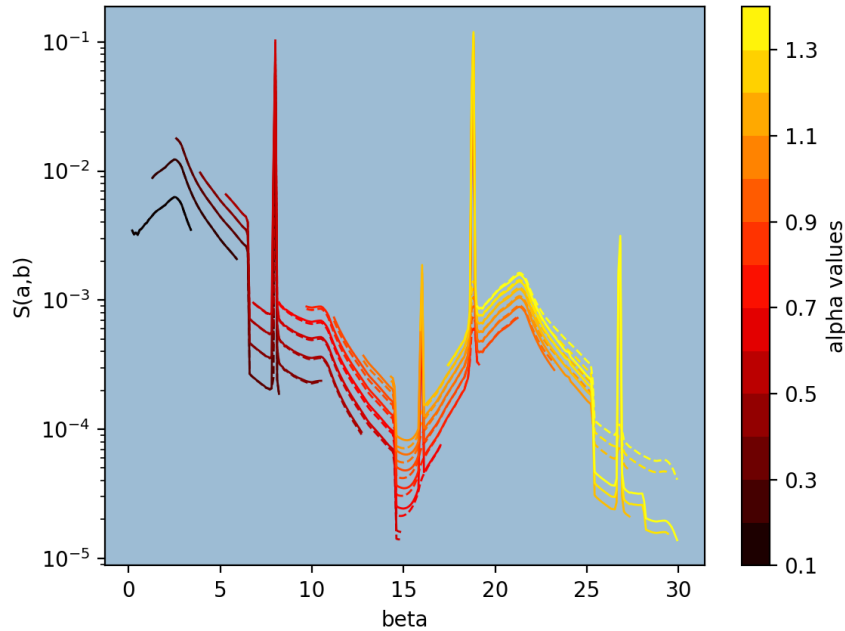

Figure 2.7: $S(\alpha, \beta)$ generated from the translated LEAPR is plotted above, where the discrete oscillator and thin triangle representations are shown using dotted and solid lines, respectively.

In viewing the differences between the continuous-representation vs. discrete oscillator $S(\alpha, \beta)$ results, it is interesting to note that the behavior is most similar at the $\beta = 7.99, 18.79$ peaks, which correspond to the 0.204 and 0.4792 eV oscillators.

Looking at Fig. 2.8, it is apparent that the continuous representation of the peak has a wider spread than that of the discrete oscillator. This is to be expected, since the triangle needs three points in the frequency distribution to define its shape, while the δ function is defined at one particular point.
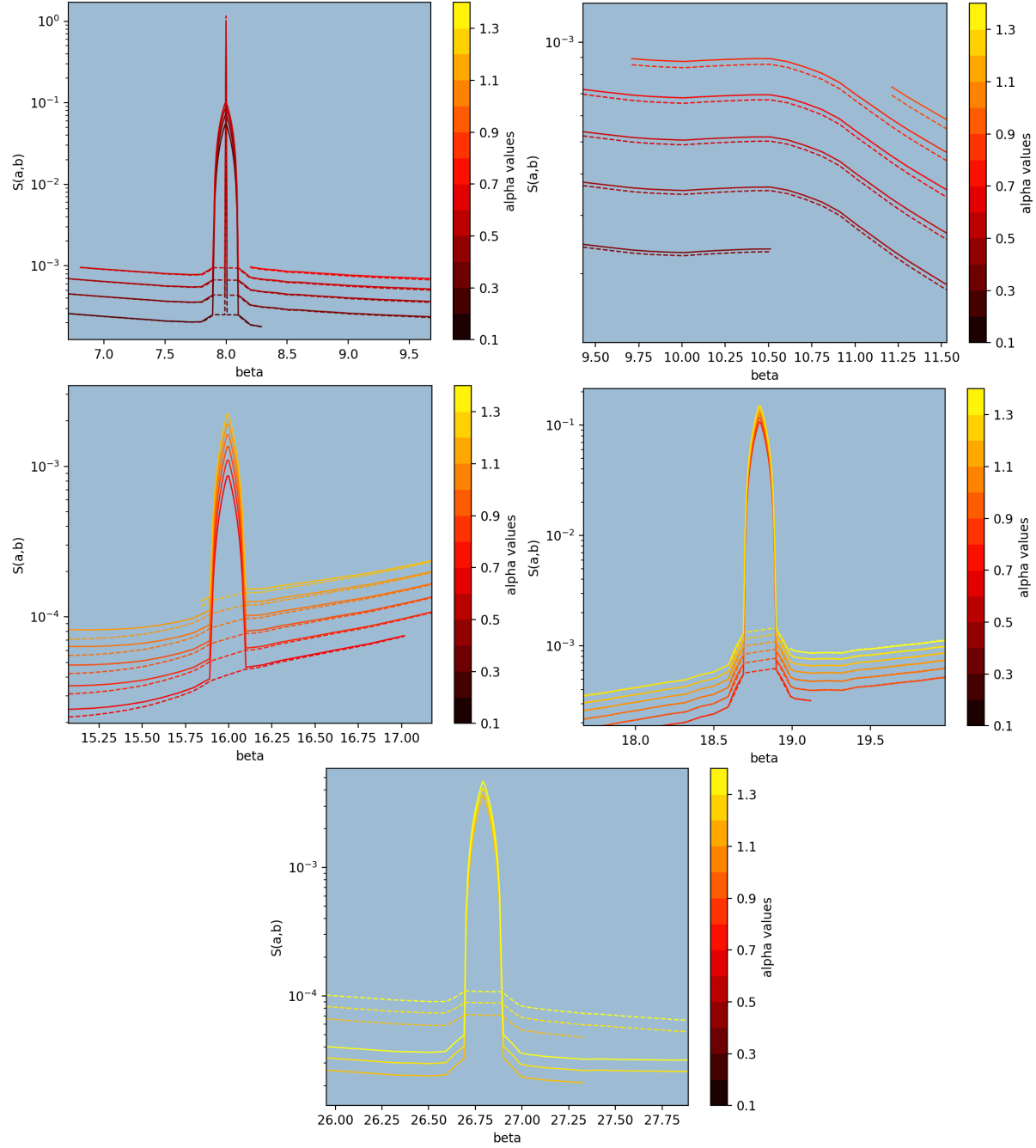
Figure 2.8: $S(\alpha, \beta)$ generated from the translated LEAPR is plotted above, where the discrete oscillator and thin triangle representations are shown using dotted and solid lines, respectively. These are close-up views of Fig. 2.7.

2.3.2 $S(\alpha, \beta)$ Response to Changes in Triangle Size

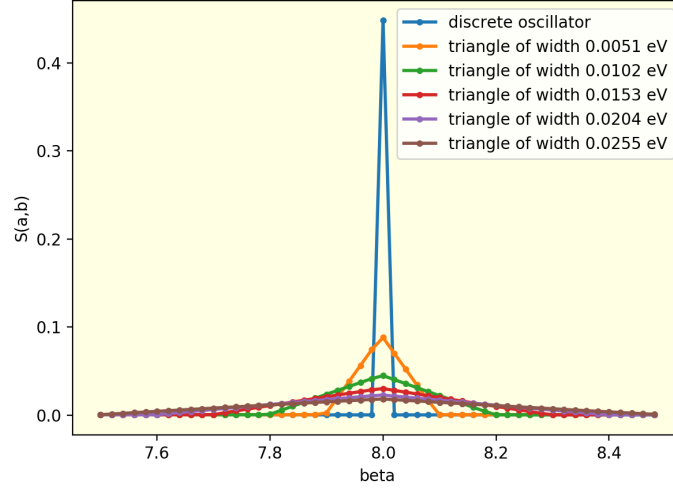## Results: Triangles of Various Widths vs. δ Func.

Figure 2.9:

We also look at the total error.

$$E_{total} = \sum_{\beta} \sum_{\alpha} \left| S^{\delta}(\alpha, \beta) - S^{\triangleleft}(\alpha, \beta) \right|$$
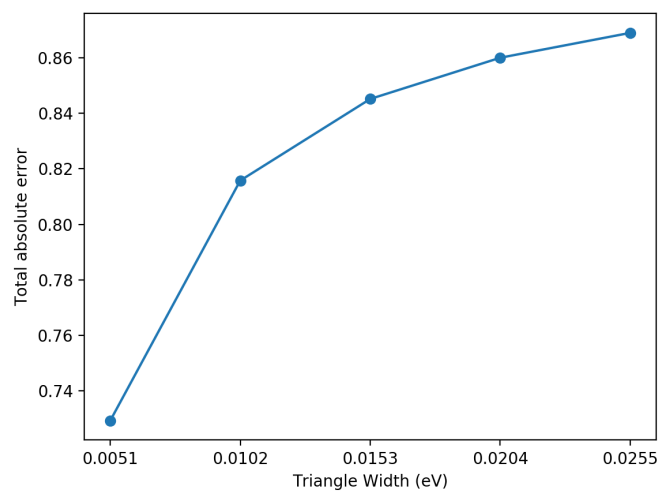
Figure 2.10: Note that as the width of the triangle decreases, the total accumulated error decreases significantly.

2.4 Nonuniform Phonon Distribution Energy Grid

Chapter 3

Improved Sampling of $S(\alpha, \beta)$

This is where I'm going to talk about Pavlou's paper

Bibliography

[1] M Herman, Cross Sections Evaluation Working Group, et al. *ENDF-6 Formats Manual Data Formats and Procedures for the Evaluated Nuclear Data File ENDF/B-VI and ENDF/B-VII*. Tech. rep. Brookhaven National Laboratory (BNL) National Nuclear Data Center, 2009.

[2] *ADS Nuclear Data Library. ACE formatted Library for Accelerator Driven Systems*. https://www-nds.iaea.org/adsV1/adsace.html. [Online; accessed 7-December-2017]. 2005.

[3] Robert Macfarlane et al. *The NJOY Nuclear Data Processing System, Version 2016*. Tech. rep. Los Alamos National Laboratory (LANL), 2017.

[4] Jesse Curtis Holmes. "Monte Carlo Calculation of Thermal Neutron Inelastic Scattering Cross Section Uncertainties by Sampling Perturbed Phonon Spectra". PhD thesis. North Carolina State University, 2014.

[5] George H Vineyard. "Scattering of slow neutrons by a liquid". In: *Physical Review* 110.5 (1958), p. 999.

[6] JI Marquez Damian, JR Granada, and DC Malaspina. *CAB models for water: a new evaluation of the thermal neutron scattering laws for light and heavy water in ENDF-6 format*. Tech. rep. 2014, pp. 280–289.

[7] PA Egelstaff and P Schofield. "On the evaluation of the thermal neutron scattering law". In: *Nuclear Science and Engineering* 12.2 (1962), pp. 260–270.

Appendices

Appendix A

Background

A.1 $T_n(\beta)$ Representation as a Convolution Integral

$$\mathcal{T}_n(\beta) = \frac{1}{2\pi} \frac{1}{\lambda_s^n} \int_{-\infty}^{\infty} e^{i\beta\hat{t}} \left[\int_{-\infty}^{\infty} P(\beta') e^{-\beta'/2} e^{-i\beta'\hat{t}} \, d\beta' \right]^n \, d\hat{t}. \tag{A.1}$$

$$\mathcal{T}_n(\beta) = \frac{1}{2\pi} \frac{1}{\lambda_s^n} \int_{-\infty}^{\infty} e^{-i\beta\hat{t}} \left[\int_{-\infty}^{\infty} P(\beta') e^{\beta'/2} e^{-i\beta'\hat{t}} \, d\beta' \right] \left[\int_{-\infty}^{\infty} P(\beta'') e^{-\beta''/2} e^{-i\beta''\hat{t}} \, d\beta'' \right]^{n-1} d\hat{t} \tag{A.2}$$

$$\mathcal{T}_n(\beta) = \frac{1}{2\pi} \frac{1}{\lambda_s^n} \int_{-\infty}^{\infty} \int_{-\infty}^{\infty} e^{-i\beta\hat{t}} P(\beta') e^{\beta'/2} e^{-i\beta'\hat{t}} \left[\int_{-\infty}^{\infty} P(\beta'') e^{-\beta''/2} e^{-i\beta''\hat{t}} \, d\beta'' \right]^{n-1} d\beta' \, d\hat{t} \tag{A.3}$$

$$\mathcal{T}_n(\beta) = \frac{1}{2\pi} \frac{1}{\lambda_s^n} \int_{-\infty}^{\infty} e^{-i\beta\hat{t}} P(\beta') e^{\beta'/2} \int_{-\infty}^{\infty} e^{-i\beta'\hat{t}} \left[\int_{-\infty}^{\infty} P(\beta'') e^{-\beta''/2} e^{-i\beta''\hat{t}} \, d\beta'' \right]^{n-1} d\hat{t} \, d\beta' \tag{A.4}$$

$$\mathcal{T}_n(\beta) = \frac{1}{2\pi} \frac{1}{\lambda_s^n} \int_{-\infty}^{\infty} P(\beta') e^{\beta'/2} \left[\int_{-\infty}^{\infty} e^{i(\beta-\beta')\hat{t}} \left[\int_{-\infty}^{\infty} P(\beta'') e^{-\beta''/2} e^{-i\beta''\hat{t}} \, d\beta'' \right]^{n-1} d\hat{t} \right] d\beta' \tag{A.5}$$

$$\mathcal{T}_n(\beta) = \int_{-\infty}^{\infty} \frac{P(\beta') e^{\beta'/2}}{\lambda_s} \left[\frac{1}{2\pi\lambda_s^{n-1}} \int_{-\infty}^{\infty} e^{i(\beta-\beta')\hat{t}} \left[\int_{-\infty}^{\infty} P(\beta'') e^{-\beta''/2} e^{-i\beta''\hat{t}} \, d\beta'' \right]^{n-1} d\hat{t} \right] d\beta' \tag{A.6}$$

$$\mathcal{T}_n(\beta) = \int_{-\infty}^{\infty} \frac{P(\beta') e^{\beta'/2}}{\lambda_s} \mathcal{T}_{n-1}(\beta - \beta') \, d\beta' \tag{A.7}$$

$$\mathcal{T}_n(\beta) = \int_{-\infty}^{\infty} \mathcal{T}_1(\beta') \mathcal{T}_{n-1}(\beta - \beta') \, d\beta' \tag{A.8}$$